Journal of Power Sources 183 (2008) 257–259

Contents lists available at ScienceDirect

Journal of Power Sources

journal homepage: www.elsevier.com/locate/jpowsour

Short communication

Orthogonal flow membraneless fuel cell

Joel R. Hayes, Allison M. Engstrom, Cody Friesen*

School of Materials, Arizona State University, PO Box 878706, Tempe, AZ 85287-8706, United States

ARTICLE INFO

Article history:
Received 26 March 2008
Received in revised form 16 April 2008
Accepted 17 April 2008
Available online 3 May 2008

Keywords:
Membraneless fuel cell
Orthogonal flow
Hydrogen
Methanol
Alkaline

ABSTRACT

This communication reports the development and performance of a membraneless fuel cell that utilizes a convective electrolyte flow orthogonal to the plane of the cell electrodes. The orthogonal flow acts to convect reactants to the electrodes and as a pseudo-membrane between anode and cathode, preventing mixed potentials caused by back diffusion of oxidant onto the anode. The membraneless design allows the cell parameters to be defined by the fuel rather than the membrane. The convective electrolyte flow eliminates the mass transport limited current regime and allows the cell to run under semi-mixed conditions. Power densities as high as 46 mW cm^{-2} were achieved with both hydrogen and methanol as fuels. Methanol had a fuel utilization of 42%.

1. Introduction

A primary component of traditional fuel cells is the membrane, which ideally provides high ionic conductivity and blocks diffusive transport of the reactants across the cell. The blocking of reactant crossover prevents the cell from being chemically shorted. The membrane also serves as the supporting electrolyte for the transport of oxidized fuel ions or reduced oxidant ions. Usually, it is a solid and passive component of the cell, but can be a liquid entrained in a porous inert matrix or circulated parallel to and between the anode and cathode such as in alkaline or phosphoric acid fuel cells [1]. The nature of the membrane typically sets the operating conditions of the cell: fuel, temperature, pH, oxidant, and humidity. In the instance of proton exchange membrane fuel cells, the pH is acidic, the temperature is typically below 90 °C, and moisture management is critical to prevent the membrane from flooding or drying out. While the overwhelming volume of work in the fuel cell area deals with improving the performance of traditional devices, a relatively new body of work has emerged that eliminates the membrane altogether.

Membraneless laminar flow fuel cells (LFFCs) operate based on the parallel laminar flow of fuel laden and oxidant laden electrolytes within a micro-fluidic channel [2–6]. The channel's opposing walls, one in the fuel stream and the other in the oxidant stream are catalyst loaded to serve as the LFFC electrodes. Under laminar flow conditions the reactant containing flows mix only through diffusive processes, providing a pseudo-membrane in the channel's center [7,8]. Fuel oxidizes at the anode, diffuses across the parallel flow boundary and complexes to the reduced oxidant. While the power density obtained with LFFCs till now is less than traditional fuel cells, a working membraneless fuel cell architecture allows for the selection of the electrolyte, and hence, a broader range of possible fuels and catalyst materials. LFFCs have been demonstrated with formic acid and O_2 [9–12], formic acid and potassium permanganate [8,11], H_2 and O_2 [5], methanol and O_2 [3], and VO^+/V^{2+} [13]. In each of these cases the operating parameters were selected to optimize the activity of the fuel and oxidant used. The early LFFCs used oxygen saturated aqueous flows and had fairly low power densities of 0.1–12 mW cm^{-2} and low fuel utilization of ~1% [3,4,10]. Integrating a more traditional air cathode gas diffusion layer created a more substantial 26 mW cm^{-2} with ~8% fuel efficiency [6]. Kjeang et al. developed a design with a 3D array of graphite rods within the laminar flow which served as both the anode and cathode in a VO^+/V^{2+} cell and increased the power density and fuel efficiency to 35 mW cm^{-2} and 63%, respectively [13].

One constraint associated with the LFFC is that the oxidized fuel must have a higher diffusivity than both the unoxidized fuel and unreduced oxidant to prevent excessive crossover and parasitic losses. Also, to minimize parasitic losses due to diffusive crossover of reactants, the length of channels must be limited, creating challenges for fuel utilization. Previously we reported the development of a radial laminar membraneless fuel cell which addressed these issues [14]. This present work moves the membraneless fuel cell beyond the laminar regime and improves both the power density and fuel utilization.

* Corresponding author. Tel.: +1 480 965 3954; fax: +1 480 727 9321.
E-mail address: CFriesen@asu.edu (C. Friesen).

0378-7753/$ – see front matter © 2008 Elsevier B.V. All rights reserved.
doi:10.1016/j.jpowsour.2008.04.061

2. Experimental details

Two types of systems were built to evaluate the performance of the orthogonal flow fuel cell, one for dissolved H_2/O_2, the other for methanol and O_2 gas. Both systems were built around the design shown in Fig. 1a, with a porous anode separated by a gap from a porous cathode. An electrolyte containing fuel flows into and through the porous anode where it is oxidized, continues across a small gap separating the electrodes, and into the porous cathode where an oxidant is injected radially. Convective electrolyte flow through the gap between the two electrodes prevents mixing of the fuel and oxidant on any single electrode. The oxidant is reduced at the cathode, and combines with the ions which were oxidized as they passed through the anode.

One system was built for sulfuric acid and dissolved H_2/O_2. 1.8 M H_2SO_4 was contained in 1 l Teflon lined stainless steel cylinders attached to variable flow Optos sapphire piston pumps (Eldex, Napa, CA) with flow rates from 0.04 to 80 ml min^{-1}. Heating elements, monitored with Teflon coated K-type thermocouples, heated the electrolyte to the desired temperature. H_2 gas was sparged into one tank through a Teflon tube, and O_2 gas was sparged into the second tank. After saturating for approximately 30 min the H_2 saturated solution was pumped into the anode inlet, and the O_2 saturated solution into the cathode. The pressure drop across the cell was ~20 psi. Both the anode and the cathode were made by punching 0.95 cm diameter discs from carbon fiber Toray paper (E-Tek, Somerset, NJ), and applying Pt black mixed with water. The Toray paper discs were dried on a hot plate, and the Pt black adhered to the surface of the carbon fibers. This procedure was adopted to avoid the hydrophobic surface normally used in GDLs made with standard Nafion/PTFE solutions. The cell was machined from a block of PEEK, and the anode and cathode were placed in PEEK holders which threaded into the main cell block. Pt wires connected to the electrodes provided electrical contact through small holes drilled into the PEEK block. The gap diameter was 0.64 cm.

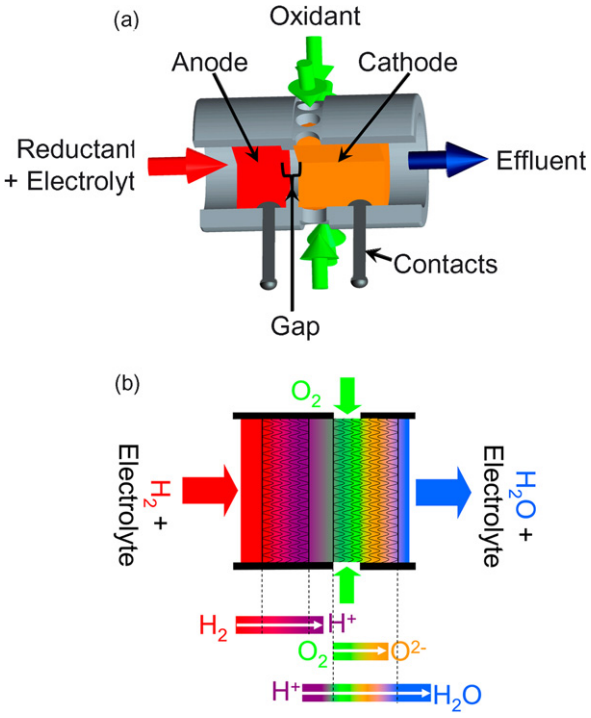

Fig. 1. (a) A schematic of the basic cell design consisting of a porous anode separated by a gap from a porous cathode. (b) Electrolyte flow transports a reductant (H_2) into the anode where it is oxidized (H^+) and transported across the gap into the porous cathode. An oxidant (O_2) is injected into the cathode, is reduced (O^{2-}), and combines with the oxidized reductant. The electrolyte flow across the gap prevents backflow and cross contamination of the reactants. The color gradient represents the reaction progression through the cell.

The second system was designed to operate on alkaline electrolytes with methanol as a fuel. A heated closed loop electrolyte pumping system was built with nickel and Monel tubing and fittings. The methanol fuel (in 1 M KOH) was contained in a 100 ml Teflon lined steel tank attached to an Optos sapphire piston pump. The fuel was maintained at room temperature to minimize evaporation, and pumped into the electrolyte stream before it reached the anode. The fuel stream flow rate was always at least a factor of 10 times smaller than the electrolyte flow to prevent a temperature decrease before the electrolyte entered the cell. The total pressure drop through the cell was ~10 psi. A Micropump (Vancouver, WA) PEEK gear pump with an adjustable flow rate of 20–180 ml min^{-1} pumped the electrolyte from the tank, through the cell, and back into the tank. N_2 flowing through a nickel sparging tube into the tank deaerated the solution. Typically 1 l of 5 M KOH electrolyte was used. O_2 gas controlled by a flow meter was directed through a Watlow Cast-X 1000 heating block, controlled with a Watlow PID temperature controller. The O_2 gas was heated to a temperature of 90 °C before flowing into the cell. The gap was set to 5 mm, and thin walled Teflon tubes of 1 mm diameter were placed lengthwise in the gap to prevent large O_2 bubbles from forming in the gap and breaking the circuit as well as causing O_2 crossover to the anode, leading to mixed potentials. The anode and cathode were made from nanoporous dealloyed Pt and Au, respectively, as detailed in Section 3. The electrode and gap diameters were 0.64 cm. A flexible heating tape placed along all tubing, valves, and the cell maintained the electrolyte at a constant temperature during operation.

The performance of the cells was evaluated using a commercial potentiostat (Gamry G750, Warminster, PA) in a two electrode configuration. To test the cell, once the fuel and oxidant streams were flowing, the open circuit potential (OCP) was measured, and then the potential was cycled from the OCP down to 0 mV (short circuit conditions) and the current response was measured. Cyclic voltammetry scans were performed at 100 mV s^{-1}.

3. Results

The reaction progression for saturated H_2/O_2 in 1.8 M sulfuric acid electrolyte is illustrated in Fig. 1b. H_2 dissolved in the electrolyte enters the porous anode, where it oxidizes to H^+. These protons are convected across the gap and enter the porous cathode, where they are joined by an orthogonally injected flow of electrolyte saturated with O_2. The O_2 reduces on the cathode to O^{2-} where it combines with the protons to form water before leaving the cell with the electrolyte flow.

Fig. 2a shows the polarization curve for dissolved H_2/O_2 in 1.8 M H_2SO_4. The electrolyte was contained in two separate vessels heated to 60 °C and saturated with H_2 and O_2 gas by bubbling. Pumps drove the two electrolytes through the cell to a waste tank. An OCP of 950 mV was obtained under low flow conditions. Under load, the power output has an optimal flow rate, with power increasing with flow rate until a mixed potential is generated at the cathode due to unoxidized fuel passing through the anode and reaching the cathode. In Fig. 2a an OCP of 865 mV was achieved with flow rates of 80 ml min^{-1}. The maximum power density reached was 45 mW cm^{-2} at 460 mV.

The polarization characteristics for the 5 M KOH methanol/O_2 gas system are shown in Fig. 2b. The primary electrolyte was deaerated with N_2, heated to 90 °C, and convection was provided at a flow rate of 40 ml min^{-1}. The fuel solution consisted of 10 mM methanol

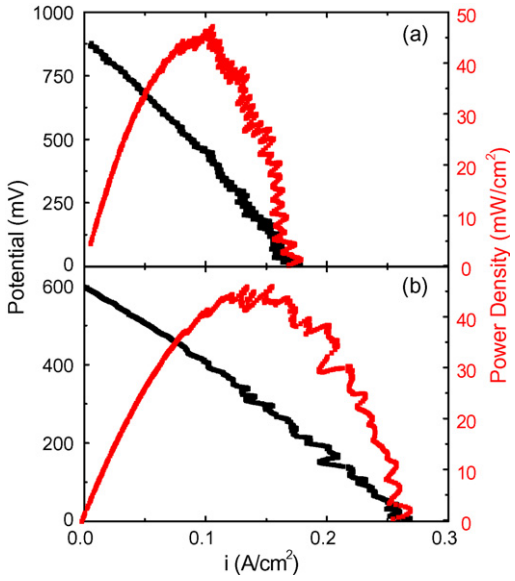

Fig. 2. Polarization and power curves for membraneless fuel cells operating on (a) dissolved H_2 and dissolved O_2 in 1.8 M H_2SO_4 at 60 °C and (b)methanol and O_2 gas in 1 M KOH at 90 °C.

in 1 M KOH at room temperature and was supplied at 1 ml min^{-1}. The fuel solution was injected into the primary electrolyte just up stream of the anode. O_2 gas was used as a reductant instead of electrolyte saturated with O_2. It was injected radially into the porous cathode just after the gap. The anode for this system consisted of particles (~0.5 mm) of $Pt_{25}Cu_{75}$ alloy which were dealloyed to produce nanoporous Pt with pore sizes on the order of 3 nm [15]. 0.25 g of Pt were placed in a 0.5 cm long, 0.64 cm diameter Teflon tube capped by carbon fiber paper discs. The nanoporous Pt enabled more complete oxidation of methanol by increasing the residence time of reaction intermediates within the pores. The cathode was nanoporous Au formed by dealloying a $Au_{25}Ag_{75}$ alloy, with pores on the order of 60 nm [16] and held the same way in a Teflon tube. Au has high O_2 reduction activity in alkaline solutions and has limited activity for methanol oxidation [17]. Those conditions yielded an open circuit potential of 600 mV and a maximum power density of 46 mW cm^{-2} at 300 mV. Since the fuel was injected at a constant rate the fuel consumption efficiency varied with total current drawn. At maximum power density, the fuel utilization was 42%.

4. Discussion

For the two chemistries reported several key attributes become apparent. When the cell is operated in the semi-mixed reactant configuration, the anode is selected for fuel oxidation activity and the cathode is chosen for O_2 reduction selectivity. Many studies have been done on mixed reactant fuel cells, where both catalysts are selective. However, it is difficult to find truly selective catalysts for both oxidation and reduction reactions and still maintain high activity. The methanol/O_2 gas cell in KOH approaches the semi-mixed condition since Au is a poor methanol catalyst, yet has high O_2 reduction activity in alkaline electrolytes. Under these conditions a significant excess of fuel may be supplied with the unused fuel consumed during the recirculation of the primary electrolyte. In the case of the H_2/O_2 cell, it is critical to control the fuel concentration and electrolyte flow rate as a function of the current density to ensure the near complete oxidation of fuel as it passes through the anode and to avoid a significant mixed potential condition at the cathode. Another interesting observation is the form of the polarization plots, which lack the traditional mass transport limited regime as the cell reaches short circuit conditions. Since the fuel and oxidant are delivered convectively to the surface of the catalyst, and not by diffusive transport, as is the case for both membrane cells and laminar flow-based micro-fluidic cells, the mass transport limited regime is not observed.

5. Conclusion

The orthogonal flow fuel cell reported here provides a unique architecture for the elimination of the membrane. The defined electrolyte flow orthogonal to the plane of the electrodes provides a pseudo-membrane, preventing oxidant from reaching the anode. With flexibility in the choice of electrolyte, the operating conditions are tuned to the fuel of choice. The current work also allows the fuel cell to run under semi-mixed conditions, and enhances mass transport of the reactants to the anode and cathode. Additionally, the cell does not require laminar flow conditions to operate, indicating that larger cells are possible as long as they are designed to prevent back flow of oxidant onto the anode and ensure complete mixing of the reductant with the oxidized fuel stream in the cathode. Power densities of 46 mW cm^{-2} were observed in this new architecture, and higher power densities are likely possible with optimization.

6. Supporting information available

Detailed description of system design and testing procedures.

Acknowledgment

The authors gratefully acknowledge the funding support of TN2.

References

[1] L. Carrette, K.A. Friedrich, U. Stimming, Chem. Phys. Chem. 1 (2000) 162–193.
[2] R. Ferrigno, A.D. Stroock, T.D. Clark, M. Mayer, G.M. Whitesides, J. Am. Chem. Soc. 124 (2002) 12930–12931.
[3] E.R. Choban, J.S. Spendelow, L. Gancs, A. Wieckowski, P.J.A. Kenis, Electrochim. Acta 50 (2005) 5390–5398.
[4] E.R. Choban, P. Waszczuk, P.J.A. Kenis, Electrochem. Solid-State Lett. 8 (2005) A348–A352.
[5] J.L. Cohen, D.J. Volpe, D.A. Westly, A. Pechenik, H.D. Abruna, Langmuir 21 (2005) 3544–3550.
[6] R.S. Jayashree, L. Gancs, E.R. Choban, A. Primak, D. Natarajan, L.J. Markoski, P.J.A. Kenis, J. Am. Chem. Soc. 127 (2005) 16758–16759.
[7] M.H. Chang, F. Chen, N.S. Fang, J. Power Sources 159 (2006) 810–816.
[8] M.H. Sun, G.V. Casquillas, S.S. Guo, J. Shi, H. Ji, Q. Ouyang, Y. Chen, Microelectron. Eng. 84 (2007) 1182–1185.
[9] R.S. Jayashree, M. Mitchell, D. Natarajan, L.J. Markoski, P.J.A. Kenis, Langmuir 23 (2007) 6871–6874.
[10] J.L. Cohen, D.A. Westly, A. Pechenik, H.D. Abruna, J. Power Sources 139 (2005) 96–105.
[11] E.R. Choban, L.J. Markoski, A. Wieckowski, P.J.A. Kenis, J. Power Sources 128 (2004) 54–60.
[12] A. Li, S.H. Chan, N.T. Nguyen, J. Micromech. Microeng. 17 (2007) 1107–1113.
[13] E. Kjeang, J. McKechnie, D. Sinton, N. Djilali, J. Power Sources 168 (2007) 379–390.
[14] K.S. Salloum, J.R. Hayes, C. Friesen, J.D. Posner, J. Power Sources 180 (2008) 243–252.
[15] D.V. Pugh, A. Dursun, S.G. Corcoran, J. Mater. Res. 18 (2003) 216–221.
[16] J. Erlebacher, M.J. Aziz, A. Karma, N. Dimitrov, K. Sieradzki, Nature 410 (2001) 450–453.
[17] J.T. Zhang, P.P. Liu, H.Y. Ma, Y. Ding, J. Phys. Chem. C 111 (2007) 10382–10388.